

# STIS CCD Imaging Throughputs

---

Charles R. Proffitt  
October 27, 2004

---

## ABSTRACT

*The results of on-orbit measurements of the STIS/CCD imaging throughputs are reported. Wavelength-dependent aperture corrections and revisions to detector and filter throughput curves are presented. The throughput of the F28X50LP filter is found to be close to pre-launch estimates. Initial on-orbit measurements of this filter had suggested a 28% lower throughput, but we find instead that the overall sensitivity of the STIS CCD itself needed to be decreased by as much as 18% at long wavelengths. Wavelength-dependent aperture corrections are also important for the reddest stars, with as much as 20% of the flux outside of a 0.5" radius.*

---

## Introduction

The Space Telescope Imaging Spectrograph (STIS) was installed in the *Hubble Space Telescope (HST)* in 1997, as part of the second HST Servicing Mission (SM2). During the subsequent Servicing Mission Orbital Verification period (SMOV2), the measured count rates in F28X50LP images were uniformly low by about 28% with no apparent color dependence (Ferguson et al. 1999). In response, the pre-launch F28X50LP throughput was reduced by 28% over most of its wavelength range. This reduced throughput F28X50LP curve was the version implemented in the **synphot**<sup>1</sup> file `stis_f28x50lp_005_syn.fits` and the calstis pipeline reference file `jba1538mo_apt.fits`. The prelaunch 50CCD throughput curve (combined detector and mirror throughputs are tabulated in the **synphot** file `stis_mirvis_006_syn.fits` and are folded together with the OTA throughput in the

---

1. See Bushouse and Simon (1998) for a description of the **synphot** synthetic photometry package.

pipeline file `h7o0858mo_pht.fits`) gave correct results for GD 71, a hot white dwarf standard star, but there was no appropriate data to determine the color dependence of the CCD imaging modes. Here, we discuss revisions made in 2001 to these throughputs based on additional data obtained during cycles 7, 8, 9, and 10.

## Relative Filter Throughputs

As STIS has both spectrographic and imaging capabilities, the on-axis throughput of any of its filters as a function of wavelength can easily be checked by comparing slitless spectra taken through clear and filtered apertures. In April 1998, as part of the calibration program 7661, such slitless spectra were taken of the hot standard star BD +75°325, using the STIS G230LB, G430L, and G750L gratings through the F28X50LP, F28X50OII, and F28X50OIII filters as well as through the unfiltered 50CCD aperture. CCD spectra were also taken using a number of MAMA filters to directly measure those filters' redleaks. The F28X50OIII filter's redleak extends to wavelengths longer than 10200 Å, where overlap of the second order spectrum prevents accurate calibration of the G750L grating; as a result of this, the long-wavelength behavior of this redleak is poorly constrained.

**Table 1.** Slitless Spectra used for measuring relative throughputs of CCD imaging filters.

Aperture	Grating	cenwave (Å)	exposure times (s)	data set name
50CCD	G230LB	2375	6	o4om010s0
F28X50OII	G230LB	2375	720	o4om010t0
F28X50OIII	G230LB	2375	720	o4om010u0
50CCD	G430L	4300	5	o4om01010
F28X50LP	G430L	4300	84	o4om01090
F28X50OII	G430L	4300	84	o4om010a0
F28X50OIII	G430L	4300	66	o4om010b0
50CCD	G750L	7751	18	o4om010d0
F28X50LP	G750L	7751	60	o4om010g0
F28X50OII	G750L	7751	720	o4om010h0
F28X50OIII	G750L	7751	600	o4om010i0
50CCD	G750L	8975	20	o4om010k0
F28X50LP	G750L	8975	50	o4om010n0
F28X50OII	G750L	8975	671	o4om010o0
F28X50OIII	G750L	8975	720	o4om010p0

To derive the throughput for each filter, the net counts observed through that filter are divided by the net counts observed for the corresponding observation through the clear

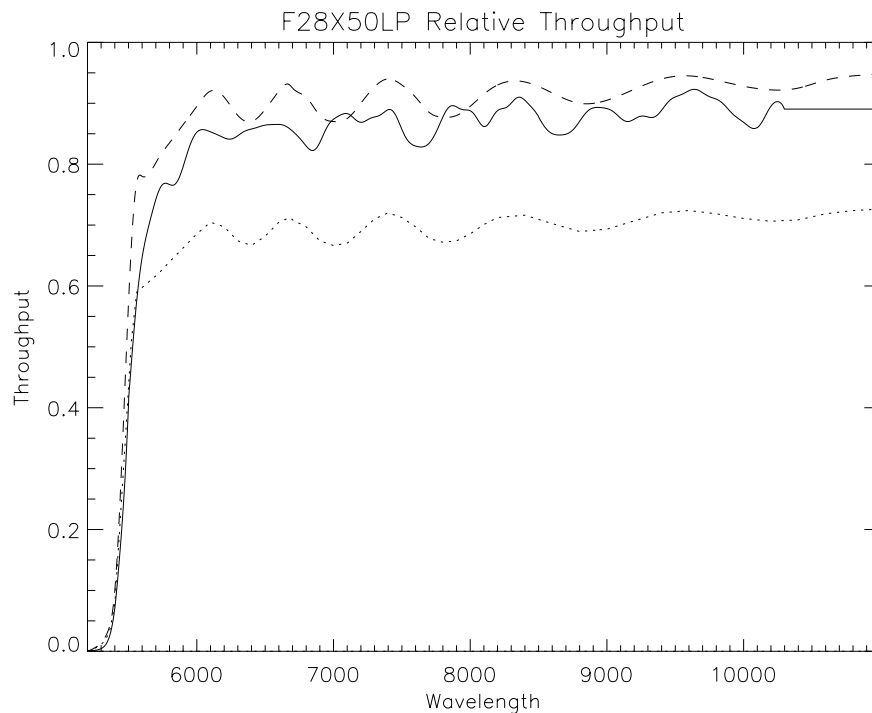
50CCD aperture. Those observations in which sufficiently strong stellar lines are observed, are shifted in the dispersion direction to align with the 50CCD observation prior to the division. Such shifts could only be cleanly measured in some of the G430L observations. For the F28X50LP observations in the G430L a shift of 1 pixel between the clear and filtered spectra was found, while for the F28X50OII and F28X50OIII filters shifts of two pixels gave the best alignment of the observed central wavelengths with the vendor specifications.

The well known near-IR fringing within the STIS CCD (Goudfrooij et al. 1998; Goudfrooij & Christensen 1998) clearly affects the G750L observations listed in Table 1. Attempts to use the long-slit fringe flats taken during this visit to remove these produced less than satisfactory results, with different scalings of the amplitudes of the fringe pattern being needed for different wavelength intervals in the same observation. This may reflect the difference between long slit and point source fringe patterns. Fortunately, we are only interested in the ratio of fluxes between observations, and the fringe pattern does not change drastically between adjacent observations taken at the same grating position. So we simply divided the spectra without first removing the fringing pattern. For this case, the same shift that gave good alignment of the stellar lines also gave good alignment of the fringes.

While the G430L spectrum does not resolve the extremely narrow band width of the F28X50OIII filter, it *can* be used to estimate the filter's equivalent width. If we exclude the uncertain red leak in the F28X50OIII filter, and consider only wavelengths  $< 6000 \text{ \AA}$ , these observations give a total equivalent width of  $4.64 \text{ \AA}$  or about 1.7% larger than that calculated from the currently tabulated pipeline throughput for this filter. The F28X50OII filter equivalent width is found to be  $34.10 \text{ \AA}$  or 1.2% larger than the pipeline throughput.

The measured F28X50LP throughput is shown in Figure 1, and, surprisingly, is nearly as high as the prelaunch estimate. We will adopt the throughput as measured by the slitless spectroscopy as the correct one and seek another explanation for the low observed count rates in the F28X50LP filter.

**Figure 1:** The dashed line shows the prelaunch throughput estimate for the F28X50LP filter and the dotted line shows the revision initially adopted following the result of lower-than-expected count rates seen in the F28X50LP filter by Ferguson et al. (1999). The solid line shows the on-orbit throughput measurement from the slitless spectroscopy described in this report. This revised throughput curve was installed in the **CALSTIS** pipeline and in **synphot** tables in July 2001.



## Absolute Imaging Throughputs

### *Adopted Spectral Energy Distributions*

To test the throughput for the STIS imaging modes, standard stars with a range of colors and accurately known spectral energy distributions (SEDs) are needed. However, a number of the stars used here were originally chosen for their utility as PSF standards rather than as good photometric standards. As a result, they don't all have SEDs measured to better than a few percent accuracy, and some imaging data was taken using subarrays which were too small to check the aperture corrections in the very far wings. The adopted SEDs we will use here are a combination of STIS spectrophotometry, Calibration Data Base System (CDBS) calspec and calobs calibration standard files, and data from other sources as needed. For the hot standards GD 71, AGK +81°266, Feige 34, and GRW +70°5824 (=EGGR 102) we have adopted calibration spectra based on STIS observations provided by the CDBS (Bohlin, Dickinson, and Calzetti 2001).

The white dwarf WD 0310–688 (= EGGR 21 1 = HIP 14754) was observed by IUE and also from the ground by Hamuy et al (1992; 1994). We scaled the NEWSIPS extraction of the IUE spectra by a factor of 1.06 to put them on the HST flux scale (see Colina & Bohlin 1994). Because of the concern with the normalization of the F28X50LP filter, G750L spectra together with an appropriate fringe flat were taken as part of an already planned PSF study. Apart from the vicinity of telluric lines, the fluxes measured in the Hamuy et al. spectrum agree with the fluxes observed in the STIS G750L spectrum to better than 1%.

The F star CPD  $-60^{\circ}7585$  (= SAO 255271) was originally observed as one of the PSF targets in the HDF-south campaign. Observations with the STIS G230LB, G430L, and G750L were obtained as parts of STIS/CAL programs 8842 and 8924.

The main-sequence K star CPD  $-35^{\circ}9181$  was selected because Hipparcos data shows no evidence for variability, and because its high galactic latitude should minimize the chance alignment of background objects. However, our HST data reveals that it does have a companion which is about 4.5 magnitudes fainter than and  $1''$  away from the primary star. STIS CCD spectra and images of the primary were obtained during the same visit, and the faint companion appear to have been just outside the  $52X2''$  aperture used for the spectroscopy. This second star (CPD  $-35^{\circ}9181$  B) is probably an M dwarf binary companion of the K star.

For the M dwarf BD  $-11^{\circ}3759$  (= GJ 555) both G430L and G750L spectra as well as 50CCD and F28X50LP imaging data were obtained during the same visit. This star was chosen as a PSF standard, but, as it is a known flare star, it is a questionable photometric standard. However, our imaging data show no evidence for any discernible variability, and as the imaging and spectral data were obtained within a single hour, it should be usable for our purposes.

### ***Broad-band 50CCD Clear Aperture and F28X50LP Photometry***

The broad bandpasses of the STIS 50CCD and F28X50LP apertures combined with the limited set of narrow-band filters complicates the testing of the wavelength dependence of the CCD imaging modes. In principle, the CCD's sensitivity could be checked using the measured dispersed mode sensitivities, but in practice the adopted grating throughputs are adjusted as needed to ensure that the spectroscopic sensitivities give the observed count rates for default spectral extractions of observations of standard stars. These adjustments to the grating throughputs, therefore, only address changes in the overall instrumental sensitivity (e.g., optics plus detector); there is no easy way to isolate the detector sensitivity.

**Table 2.** Sources of adopted SEDs.

Target	V	B-V	Spectrum Source	Wavelength Coverage (Å)
GD 71	13.06	-0.25	calspec/gd71_stis_001.fits	1148 to 10245
AGK +81°266	12.10	-0.20	calspec/agk_81d266_stis_001.fits	1148 to 10245
Feige 34	11.0	-0.16	calspec/feige34_stis_001.fits	1148 to 10245
GRW +70°5824	12.80	-0.09	calspec/grw_70d5824_stis_001.fits	1148 to 10245
WD 0310-688	11.1	+0.05	SWP15471.MXLO+LWR11954.MXLO	1160 to 3300
			Hamuy et al. 1992; 1994	3300 to 10000
			STIS G750L O69C010X0	5240 to 10245
CPD -60°7585	10.06	+0.41	STIS G230LB O6H301090	1800 to 3150
			STIS G430L O6H3010A0	2900 to 5700
			STIS G750L O6H3010B0	5240 to 10245
			STIS G750L O69C020X0	5240 to 10245
G158-100	14.89	+0.69	calobs/g158_100_011.fits	3200 to 9200
CPD -35°9181	10.20	+0.92	STIS G230LB O6H302010	1800 to 3150
			STIS G430L O6H302020	2900 to 5700
			STIS G750L O6H3020H0	5240 to 10245
BD -11°3759	11.35	+1.63	STIS G430L O5JA040H0	2900 to 5700
			STIS G750L O5JA040I0	5240 to 10245

Instead we have used 50CCD and F28X50LP imaging data of stars of a number of different colors, for which we have an adequate understanding of the SEDs. By comparing the observed and predicted count rates we can constrain changes to the overall sensitivity curve.

Saturated STIS data taken using the CCDGAIN = 4 setting preserves the total number of counts to high accuracy as long as the chosen aperture is large enough to include all the charge that has bled along the columns (Gilliland 1999). We have verified that this also works with our imaging data, and where possible we will give preference to large-aperture photometry on the best exposed images to determine the total imaging count rate. This should also minimize the effects of CTI degradation. We assume the ratio between gain 1 and gain 4 to be the value of  $4.08 \pm 0.05$  found by Goudfrooij (1998).

For BD -11°3759, CPD -60°7585, CPD -35°9181, and WD 310-688 we have very deep images with both the 50CCD and F28X50LP modes that can be used to directly measure the flux using an 8" radius aperture. For G158-100 we have data of similar quality for the F28X50LP mode only.

Most of our deep GRW +70°5824 images were taken using 256X256 subarrays to decrease data volume, so we only quote photometric results for apertures of 6" or less in

size (Table 20), and assume that the aperture corrections at larger radii are the same as found for WD 310–688.

The images of our hottest star, GD 71, are also too shallow to measure the far wings of the PSF. Instead we took the magnitudes measured with a 1'' aperture and applied the aperture corrections derived from our measurements of GRW +70°5824 and WD 310–688.

Detailed photometric measurements for these stars are tabulated in Appendix A, while our final adopted instrumental magnitudes are listed in Table 3.

**Table 3.** The adopted observed values for 50CCD and F28X50LP instrumental magnitudes (i.e.,  $-2.5\log_{10}(\text{count rate})$ ) for imaging sensitivity calibration stars, including aperture corrections, are given for CCDGAIN = 4, as are the **synphot** predictions for the same magnitudes, calculated assuming both the new and the old CCD sensitivity curves. The spectral type and observed  $B-V$  color of each star is also listed.

Star	Spectra	B-V	50CCD images	F28X50LP images	50CCD new pred	F28X50LP new pred	50CCD old pred	F28X50LP old pred
GD 71	DAw	-0.25	-11.975	-10.256	-11.967	-10.268	-12.007	-10.401
GRW +70°5824	DA	-0.09	-12.008	-10.556	-12.031	-10.590	-12.085	-10.724
WD 0310–688	DA	+0.05	-13.289	-11.996	-13.276	-11.975	-13.338	-12.109
CPD -60°7585	F8	+0.41	-14.508	-13.775	-14.501	-13.763	-14.600	-13.903
G158–100	DG	+0.79	...	-9.182	...	-9.168	...	-9.311
CPD -35°9181 A	K3V	+0.92	-14.474	-14.010	-14.476	-14.008	-14.598	-14.152
CPD -35°9181 B	M?	...	-10.0:	-9.7:	...	...	...	...
BD -11°3759	M4V	+1.63	-14.553	-14.342	-14.560	-14.343	-14.708	-14.497

#### *Effects of Charge Transfer Inefficiency.*

The analysis presented here was completed before correction formula for the effects of charge transfer inefficiency (CTI) on STIS photometry were derived. The assumption was that by using very deep images and large apertures, the effects of CTI losses would be minimized. Now that Goudfrooij & Kimble (2002) have published correction formula for small aperture photometry of STIS CCD imaging observations, we can check these assumptions. The deep but unsaturated images taken in programs 8422 and 8844 typically had  $10^5 e^-$  in a 5 pixel radius aperture. Goudfrooij & Kimble's calibration suggests that CTI corrections for these observations should be  $< 2\%$ .

The effects of CTI on large-aperture radius measurements are more difficult to judge as Goudfrooij and Kimble did not study such cases. However, we note that the instrumental magnitudes measured for BD -11°3759 (Table 15 in) and CPD -35°9181 (Table 18) with very large (6 to 8'' radius) apertures, show no dependence on exposure time; the mea-

sured counts agree to  $\ll 1\%$  even for a factor of 10 difference in exposure time (and exposure level). This suggests that CTI losses for these measurements were minimal, and we conclude that our results have not been significantly affected by the neglect of CTI effects. However, when analyzing less deeply exposed data, corrections for CTI effects will be essential.

*Effects of time-dependent optical throughput changes.*

STIS has also shown time-dependent sensitivity (TDS) changes that are independent of CTI effects. Mobasher, Davies, & Goudfrooij's (2004) study of the full-field CCD imaging sensitivity found that, once CTI effects were corrected for, there was no detectable change in STIS CCD imaging sensitivity. However, that study only used relatively cool stars in the globular cluster  $\omega$  Cen, while the largest changes in sensitivity are expected to be at the shortest wavelengths. In the following, we will rely on the assumption that the wavelength dependence of the TDS for CCD imaging modes follows that of the STIS CCD 1st order spectroscopic modes.

The TDS changes for spectroscopic modes have been detailed in a number of STIS ISRs, most recently Stys, Bohlin, & Goudfrooij (2004), while the TDS changes for MAMA imaging modes were discussed by Proffitt et al. (2003). To a good approximation, the TDS changes as a function of wavelength are independent of the optical element considered. Both the NUV-MAMA G230L and the CCD G230LB modes show very similar trends, while the MAMA imaging throughput changes are consistent with those found for the comparable 1st order grating modes.

If we assume that CCD imaging modes show the same time dependent sensitivity changes that were found for 1st order spectral modes by Stys et al. (2004), then we find that STIS CCD imaging TDS corrections are completely negligible ( $< 0.002$  mag), except for the case of hot stars observed with the unfiltered 50CCD mode. For the STIS imaging data considered in this ISR, the largest correction would be for our 50CCD observations of WD 310–688 made in September 2000 (Table 19), where we estimate a correction for TDS of only  $-0.0050$  mag. TDS corrections have, however, been increasing with time, and by mid 2004 the TDS correction to 50CCD photometry for sufficiently hot stars is expected to be as large as  $-0.021$  mag. The exact correction will depend on both the date of the observation and the SED of the source.

These assumed time-dependent corrections to the STIS imaging throughputs have now been made available for the STSDAS **synphot** package<sup>1</sup>, and the appropriate wavelength-dependent throughput for any date can be obtained by specifying the Modified Julian Date (MJD) in the definition of the bandpass, e.g., `band(stis,ccd,50ccd,mjd#50692)`.

---

1. The latest versions of the synphot reference files that include TDS for STIS CCD imaging modes can be obtained from [http://www.stsci.edu/resources/software\\_hardware/stsdas/synphot](http://www.stsci.edu/resources/software_hardware/stsdas/synphot). These files should be included with the STSDAS 3.3 distribution which will be released in late 2004.

This can be used, for example, in the **synphot** task **calcphot** to estimate the effect of TDS changes on imaging count rates for any assumed source SED.

#### *Aperture Corrections for Individual Stars*

The observed data can also be used to derive aperture corrections for these filters. Because of the very broad bandwidths of these filters, and the substantial red halo present at wavelengths longer than 6000 Å (see section 7.1.7 of Kim Quijano et al. 2003), the aperture corrections for both the 50CCD and F28X50LP filters depend strongly on the shape of the target's SED. In Tables 4 and 5, we list the aperture corrections derived from our photometry of the target stars. To aid observers wishing to use these tables to calculate aperture corrections for stars of any color, we also provide magnitudes and colors for these calibration stars in Table 6. These latter values were calculated using **synphot** together with the adopted SED for each star, and may differ slightly from the observed values.

**Table 4.** Measured aperture corrections for 50CCD images as a function of aperture radius in pixels, relative to a reference aperture of 8" radius.

Star	2	3	4	5	7	10	15	19.7	39.4	59.2	118
GRW +70°5824	-0.464	-0.283	-0.219	-0.183	-0.137	-0.102	-0.074	-0.057	-0.021	-0.009	
WD 310-688	-0.461	-0.276	-0.216	-0.194	-0.138	-0.105	-0.076	-0.060	-0.022	-0.010	-0.001
CPD -60°7585	-0.523	-0.314	-0.242	-0.210	-0.169	-0.130	-0.104	-0.088	-0.043	-0.024	-0.004
CPD -35°9181 A	-0.585	-0.352	-0.282	-0.244	-0.193	-0.152	-0.120	-0.102	-0.053	-0.029	-0.003
BD -11°3759	-0.806	-0.524	-0.379	-0.328	-0.280	-0.235	-0.197	-0.173	-0.104	-0.064	-0.009

**Table 5.** Measured aperture corrections for F28X50LP images as a function of aperture radius in pixels, relative to a reference aperture of 8" radius.

Star	2	3	4	5	7	10	15	19.7	39.4	59	118
GRW +70°5824	-0.621	-0.344	-0.245	-0.214	-0.166	-0.124	-0.094	-0.078	-0.036	-0.021	
WD 310-688	-0.643	-0.363	-0.262	-0.228	-0.184	-0.140	-0.109	-0.091	-0.047	-0.026	-0.004
CPD -60°7585	-0.632	-0.375	-0.288	-0.259	-0.215	-0.158	-0.127	-0.110	-0.059	-0.035	-0.005
CPD -35°9181 A	-0.662	-0.397	-0.299	-0.273	-0.225	-0.182	-0.148	-0.126	-0.074	-0.039	-0.004
BD -11°3759	-0.813	-0.535	-0.392	-0.346	-0.300	-0.251	-0.212	-0.187	-0.109	-0.068	-0.009

**Table 6.** Calculated magnitudes and colors of calibration stars.

Star	50CCD (STMAG)	F28X50LP (STMAG)	50CCD-LP (STMAG)	V	U-B	B-V	V-R <sub>c</sub>
GRW +70°5824	12.848	13.747	-0.899	12.716	-0.772	-0.057	-0.100
WD 310-688	11.603	12.361	-0.759	11.358	-0.624	0.041	-0.079
CPD -60°7585	10.378	10.574	-0.196	10.041	-0.017	0.417	0.275
CPD -35°9181 A	10.402	10.328	0.074	10.202	0.833	0.917	0.583
BD -11°3759	10.318	9.994	0.325	11.263	1.241	1.476	1.274

### *Wavelength-Dependent Aperture Corrections*

The encircled energy curves given above are based on observations of particular stars, and may be difficult to generalize for the case of arbitrary SEDs. For such cases we have developed an approximate model of the wavelength-dependent aperture corrections for the STIS CCD (Table 7). The curves for 3740 and 5007 Å are based on the observed STIS narrow band filter observations, while the curve for 1750 Å is calculated using a Tiny Tim model. At wavelengths of 6500 Å and longer, we assume that the core of the PSF can be described by a TinyTim model, and then add the halo due to the red light scattered within the CCD detector. The wavelength-dependent behavior of this halo was estimated by fitting the scattered light halo seen in a STIS G750L spectrum with a simple circularly symmetric PSF model.

To calculate the encircled energy curve for a given SED and filter combination, the wavelength-dependent encircled energy at each aperture radius in Table 7 should be convolved with the target's adopted SED and the total system throughput for the chosen observing mode.

### *Accuracy of Aperture corrections*

The aperture corrections discussed above are based on a rather limited number of very deep imaging observations. We can estimate the effects of telescope breathing on the PSF by comparing TinyTim models calculated using different focus values. These calculations suggest that focus variations of +/- 5 microns can change the 2 pixel radius throughput by as much as 0.05 mag, but this decreases to less than 0.01 magnitudes for apertures of 5 pixels or larger in radius. Repeatability results from the monitoring of the STIS full-field sensitivity (Mobasher, Davies, & Goudfrooij 2004) also show rms variations of about 0.01 mag for measurements of bright stars.

If we attempt to reproduce the results for individual observations given in Table 6 by convolving the adopted SEDs with the instrumental throughputs and the wavelength-dependent aperture corrections given in Table 7, we find agreement to within 0.02 mag. Systematic uncertainties in the details of the adopted SEDs, throughputs, and aperture cor-

rections will make it difficult to significantly improve these limits on the accuracy of the aperture corrections.

**Table 7.** Model of encircled energy fraction as a function of wavelength for STIS CCD imaging.

$\lambda$ (Å)	Fraction in central pixel	Aperture Radius in Pixels							
		2	5	10	15	19.7	39.4	59	118
1750	0.246	0.667	0.873	0.949	0.979	0.990	0.998	1.000	1.000
3740	0.283	0.704	0.857	0.920	0.945	0.960	0.994	0.999	1.000
5007	0.253	0.679	0.857	0.916	0.934	0.948	0.985	0.997	1.000
6500	0.214	0.597	0.865	0.902	0.927	0.942	0.966	0.975	0.992
7500	0.178	0.536	0.825	0.866	0.892	0.909	0.942	0.957	0.986
8500	0.141	0.463	0.748	0.799	0.827	0.848	0.897	0.924	0.973
9500	0.100	0.342	0.607	0.672	0.705	0.733	0.809	0.857	0.946
10000	0.080	0.275	0.518	0.589	0.624	0.655	0.748	0.810	0.926
10500	0.064	0.238	0.447	0.517	0.553	0.585	0.690	0.764	0.907

#### *Adopted CCD Imaging Throughput Revisions*

The STSDAS **synphot** package (Bushouse & Simon 1998) was used to calculate wavelength-dependent count rates for the 50CCD imaging mode, assuming the SEDs discussed above and the original (pre-2001) CCD imaging photometry throughput curve. These count rates were then multiplied by an adjustable wavelength-dependent correction factor (and by our revised F28X50LP throughput curve for the filtered data) and then summed to give a predicted count rate for each star and filter combination. The wavelength-dependent correction factor was then adjusted to minimize the sum of the root-mean-square (RMS) differences between the predicted and observed instrumental magnitudes. Table 8 shows the final adopted correction vector. Figure 2 depicts the dramatic improvement obtained with the revised throughput curve. Figure 3 compares the old and new CCD throughput curves. The required correction curve is close to unity up to the wavelength of the F28X50OII filter, and then decreases smoothly as a function of wavelength towards the red, dropping to 0.824 at 10400 Å. Several parameters characterizing the revised 50CCD and F28X50LP band passes are given in Table 9. The definitions of these parameters are given in Bushouse and Simon (1998) in the section describing the **bandpar** task.

***Absolute Throughput of the F28X50OII and F28X50OIII Filters***

The two narrow-band STIS CCD filters provide an independent check of the CCD imaging throughput. To check the absolute sensitivity of the CCD near 3727 Å with the F28X50OII filter we will use observations of the hot standards AGK +81°266 and GRW +70°5824 from STIS calibration programs 7079, 8422, 8506, and 8856. For F28X50OIII we will use observations of Feige 34 and GRW +70°5824 from calibration programs 7079, 8051, and 8422.

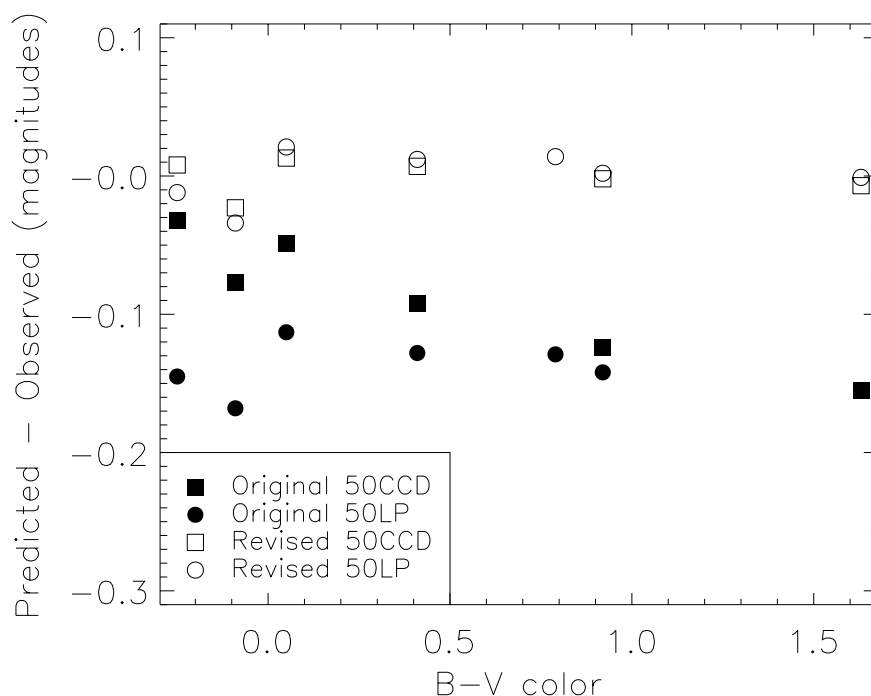
Observations of these stars in F28X50OII and F28X50OIII were of longer duration (from 90 to 1000 seconds) than the 50CCD and F28X50LP imaging observations discussed above. When performing large-aperture photometry on such data, it is especially important to remove all hot pixels and cosmic rays. We eliminated dark pixels not removed by the standard pipeline dark interactively, using the iraf **imedit** task.

To derive aperture corrections for the F28X50OII filter, we used deep coadded images (o5ja07010, o5ja07020, and o5ja07030) of another star, HD 38666, which were taken as part of STIS calibration program 8422. These are compared to aperture corrections calculated with TinyTim (Krist 1995) in Table 10. While there are substantial differences for small radii apertures, both agree that essentially all the flux should be within a 3'' aperture for this filter. For the F28X50OIII filter, we do not have any data as deep as our best [O II] data, but the best estimates from the average of the [O III] images of Feige 34 show a similar pattern; for small apertures the encircled energy is somewhat less than TinyTim predictions, and less than 0.3% of the total light falls outside a 59 pixel (3'') radius.

**Table 8.** Adopted corrections to CCD throughput curve.

Wavelength (Å)	Throughput ratio
1500.00	1.012
2625.00	1.014
3750.00	1.016
5008.00	0.940
6808.00	0.873
8608.00	0.833
10408.0	0.824

**Figure 2:** Here we compare the predicted and observed count rates for 50CCD (squares) and F28X50LP (circles) imaging of our standard stars for assuming the old (filled symbol) and the revised CCD throughputs (open symbols). For all calculated F28X50LP magnitudes in this figure, the revised F28X50LP curve is assumed. Using the old Ferguson et al (1998) F28X50LP throughput with the old CCD throughput would move the filled circles close to zero, but would of course not affect the predicted values for unfiltered 50CCD imaging.



Individual photometric measurements are tabulated in appendix A. In Table 11 and Table 12 we compare the **synphot** infinite aperture prediction to the actual counts measured using a 59 pixel (3'' radius) aperture. **Synphot** predictions are made using the currently installed CCD throughput curve and filter throughput curves and then corrected for effects of the small filter throughput changes discussed above (+1.2% for F28X50OII and +1.7% for F28X50OIII) as well as the change to the CCD sensitivity curves found above (+1.6% at 3727 Å and -6% at 5008 Å). The Feige 34 [O III] data is of considerably higher signal-to-noise than the GRW +70°5824 observation. We conclude that the count rates observed through the narrow-band filters are consistent with the throughput changes derived from the broad band 50CCD and F28X50LP photometry mentioned above.

**Figure 3:** The old (solid line) and revised (dashed line) CCD throughputs are shown. The curves shown include the effects of all STIS optics, but not those of the OTA.

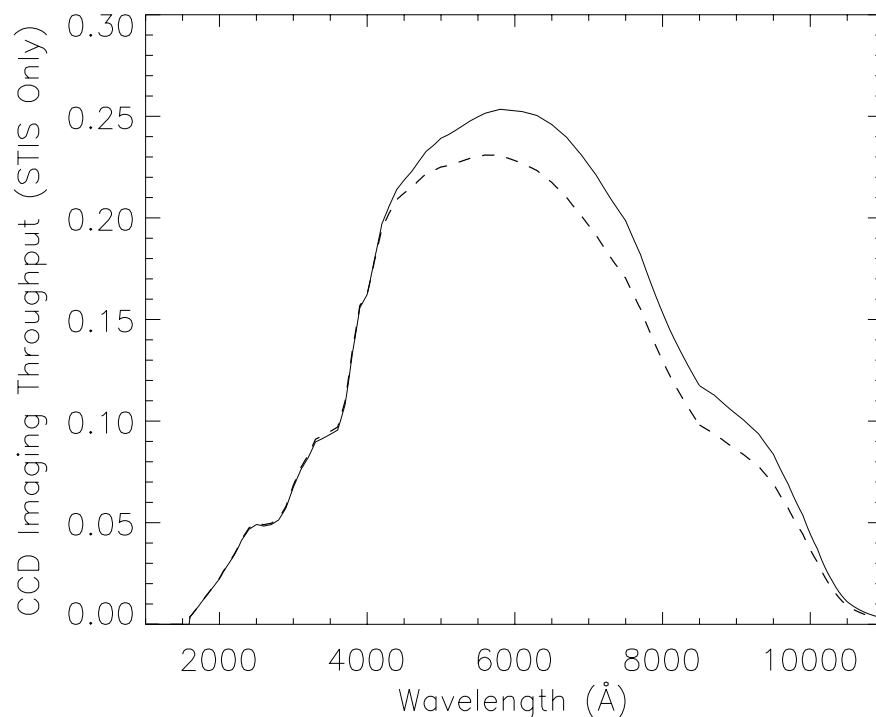


**Table 9.** Synphot bandpar results for the revised band passes when CCDGAIN = 1.

Band pass	URESP (PHOTFLAM)	PIVWV	BANDW	TPEAK	EQUVW	RECTW	EMFLX
	ergs/cm <sup>2</sup> /sec/Å	Å	Å		Å	Å	ergs/cm <sup>2</sup> /sec
50CCD	9.951E-20	5733.2	1840.0	0.1477	729.26	4937.3	5.015E-16
F28X50LP	1.640E-19	7216.7	1139.8	0.1241	365.96	2948.3	6.200E-16

**Table 10.** Aperture corrections in magnitudes for F28X50OII and F28X50OIII

PSF		Aperture radius (CCD pixels)						
Source	Filter	2.	5.	10.	15.	19.7	39.4	59.
HD 38666	F28X50OII	-0.381	-0.167	-0.090	-0.061	-0.044	-0.006	-0.001
Tinytim	F28X50OII	-0.298	-0.118	-0.054	-0.033	-0.020	-0.004	-0.001
Feige 34	F28X50OIII	-0.420	-0.167	-0.095	-0.074	-0.058	-0.016	-0.003
TinyTim	F28X50OIII	-0.369	-0.125	-0.061	-0.038	-0.028	-0.009	-0.005

**Table 11.** Comparison of F28X50OII photometry with corrected **synphot** predictions.

Star	Synphot Infinite Aperture Prediction (instrumental mag)	Observed Magnitude - Synphot Prediction (mag)
AGK +81°266 @ gain=1	-9.354	+0.014
AGK +81°266 @ gain=4.08	-7.827	-0.009
GRW +70°5824	-6.418	-0.024
Feige 34	-8.594	-0.006

**Table 12.** Comparison of F28X50OIII photometry with corrected **synphot** predictions.

star	Synphot Infinite Aperture Prediction (instrumental mag)	Observed Magnitude - Synphot Prediction (mag)
GRW+70°5824	-4.681	+0.038
Feige 34	-6.273	+0.010

Many common filter systems are normalized so that Vega has zero magnitude in all bands. *HST* also uses the STMAG system, where the magnitude is defined to be  $-2.5 \log(F_\lambda) - 21.10$ , with  $F_\lambda$  in units of  $\text{ergs}/\text{cm}^2/\text{s}/\text{\AA}$ . For the STIS CCD filters  $1 \text{ e}^-$  per second corresponds to the VEGAMAG and STMAG values given in Table 13.

**Table 13.** Magnitudes using VEGAMAG and STMAG normalizations of source producing a count rate of  $1 \text{ e}^-/\text{s}$  in each of the STIS CCD filters.

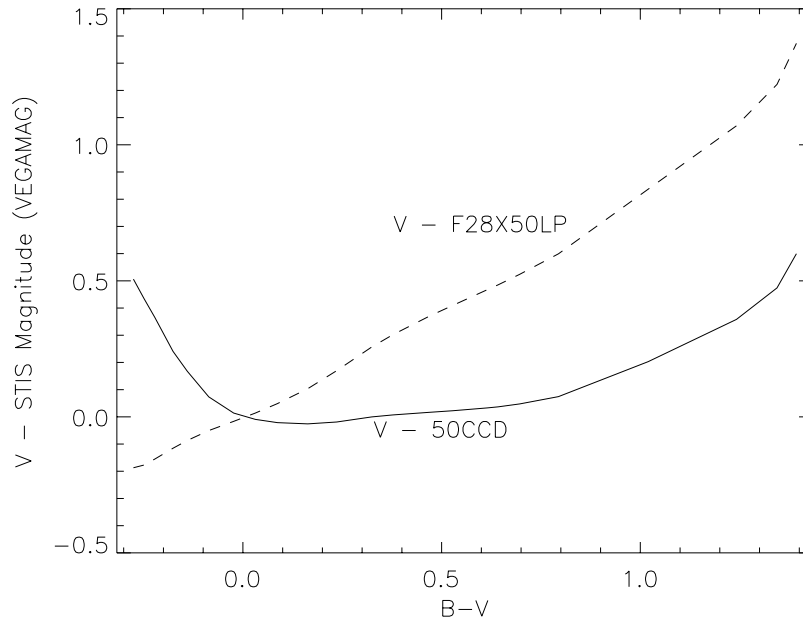
Filter	VEGAMAG	STMAG
50CCD	26.06	26.41
F28X50LP	24.99	25.86
F28X50OII	19.72	19.72
F28X50OIII	18.95	19.25

## Conversion to Johnson Colors and Magnitudes

The broad wavelength coverage of the STIS 50CCD and F28X50LP filters makes conversions to other photometric systems strongly color dependent (see Figure 4). As an example, we present in Table 14 **synphot** calculations of colors for a series of solar-abundance near-main-sequence models interpolated from the Kurucz (1993) grid. We include the magnitude difference between Johnson *V* and each of the STIS CCD filters.

Users should remember that **synphot**'s definitions of the *UBVRI* passbands are only accurate at the 5% level (see p. 17 of Bushouse and Simon 1998). Also note that the results given for the F28X50OIII filter include the effects of its poorly measured red leak.

**Figure 4:** The difference between Johnson *V* magnitudes and STIS 50CCD and F28X50LP magnitudes as a function of *B–V* color for Kurucz (1993) solar-abundance main-sequence models.



## Pipeline and Synphot Reference File Updates

The revised STIS/CCD throughput curve illustrated in Figure 3 was incorporated in a revised photometric throughput (`pht`) file for STIS/CCD imaging observations, and this file was delivered to the STScI Calibration Database System (CDBS) on July 11, 2001. Note that throughputs incorporated into the STIS `pht` files include the end-to-end throughput of the entire optical path, including the contributions from HST's Optical Telescope Assembly (OTA). A new version of the corresponding **synphot** file, `stis_mirvis_007_syn.fits`, which does not include the OTA throughput, was also delivered at this time. The throughput files for the F28X50LP filter were also corrected to reproduce the measured ratio of the slitless spectra taken with and without the F28X50LP filter in place.

**Table 14.** Johnson and STIS colors calculated for solar abundance Kurucz main-sequence models. All colors in this table use the VEGAMAG normalization.

$T_{\text{eff}}$	$\log g$	50CCD- F28X50LP	$B-V$	$V-R$	$V-50CCD$	$V-$ F28X50LP	$V-$ F28X50II	$V-$ F28x50III
40000	4.0	-0.693	-0.275	-0.130	0.506	-0.187	1.436	0.026
30000	4.0	-0.611	-0.248	-0.124	0.434	-0.177	1.313	0.012
25400	3.9	-0.521	-0.221	-0.107	0.365	-0.155	1.212	0.003
18700	3.9	-0.355	-0.175	-0.078	0.240	-0.115	0.968	-0.001
15400	3.9	-0.254	-0.139	-0.057	0.167	-0.086	0.794	-0.001
11900	4.0	-0.123	-0.085	-0.033	0.073	-0.050	0.465	-0.000
10000	4.05	-0.030	-0.023	-0.011	0.013	-0.016	0.110	-0.002
9230	4.1	0.023	0.031	0.012	-0.009	0.013	-0.049	-0.012
8720	4.2	0.069	0.086	0.041	-0.021	0.048	-0.140	-0.026
8200	4.3	0.129	0.163	0.086	-0.025	0.103	-0.192	-0.049
7700	4.3	0.188	0.236	0.139	-0.018	0.169	-0.196	-0.071
7200	4.3	0.257	0.324	0.208	0.000	0.256	-0.157	-0.089
6890	4.3	0.294	0.377	0.243	0.007	0.301	-0.188	-0.098
6440	4.3	0.353	0.469	0.295	0.016	0.370	-0.291	-0.107
6200	4.4	0.386	0.527	0.325	0.022	0.409	-0.385	-0.110
5860	4.4	0.434	0.614	0.369	0.032	0.467	-0.576	-0.111
5770	4.5	0.448	0.642	0.382	0.036	0.485	-0.654	-0.111
5570	4.5	0.476	0.696	0.412	0.047	0.524	-0.819	-0.109
5250	4.5	0.524	0.794	0.468	0.074	0.599	-1.171	-0.101
4560	4.5	0.633	1.019	0.650	0.202	0.836	-2.019	-0.093
4060	4.5	0.711	1.241	0.802	0.358	1.069	-2.510	0.017
3750	4.55	0.747	1.344	0.863	0.474	1.222	-2.597	0.238
3500	4.6	0.773	1.392	0.900	0.599	1.372	-2.694	0.521

## References

- Bohlin, R. C., Dickinson, M. E., & Calzetti, D. 2001, AJ, 122, 211
- Bohlin, R. C., & Goudfrooij, P. STIS ISR 2003-03 “An Algorithm for Correcting CTE Loss in Spectrophotometry of Point Sources with the STIS CCD”, (Baltimore: STScI).
- Bushouse, H., and Simon, B. 1998, “SYNPHOT User’s Guide”, (Baltimore: STScI).

- Colina, L., & Bohlin, R. C. 1994, Instrument Science Report on Standard Calibration Sources CAL/SCS-003.
- Ferguson, H., Smith, E., Walsh, J., Tolstoy, E., & Plait, P. 1999, "STIS Image-mode Throughputs", private communication.
- Gilliland, R. L. 1999, STIS ISR 1999-05, STIS/CCD "Time Series Photometry with Saturated Data", (Baltimore: STScI).
- Goudfrooij, P. 1998, STIS ISR 1998-31 "STIS CCD Performance Monitor: Read Noise, Gain, and Consistency of Bias correction during June 1997 - June 1998".
- Goudfrooij, P., & Kimble, R. A. 2002, "Correcting STIS CCD Photometry for CTE Loss "in HST Calibration Workshop, Space Telescope Science Institute, 2002, S. Arribas, A. Loekemoer, & B Whitmore, eds., p. 105
- Hamuy, Mario; Suntzeff, N. B.; Heathcote, S. R.; Walker, A. R.; Gigoux, P.; Phillips, M. M., 1994, PASP, 106, 566
- Hamuy, Mario; Walker, A. R.; Suntzeff, N. B.; Gigoux, P.; Heathcote, S. R.; Phillips, M. M. 1992, PASP, 104, 533
- Kim Quijano, J., et al. 2003, STIS Instrument Handbook, Version 7.0, (Baltimore: STScI).
- Kurucz, R. L. 1993, CDROM No. 13, "ATLAS9 Stellar Atmosphere Programs and 2 km/s Grid", (Cambridge: Smithsonian Astrophys. Obs.)
- Krist, J. 1995, "Simulation of HST PSFs using Tiny Tim", in Astronomical Data Analysis Software and Systems IV, ASP Conference Series, Vol. 77, 1995, R.A. Shaw, H.E. Payne, and J.J.E. Hayes, eds., p. 349.
- Mobasher, B., Davies, J., & Goudfrooij, P. 2004, STIS ISR 2004-03, "Full-Field Sensitivity of STIS CCD Imaging and its Temporal Dependence".
- Proffitt, C. R., Brown, T. M., Mobasher, B., & Davies, J., 2003, STIS ISR 2003-01, "Absolute Flux Calibration of STIS MAMA Imaging Modes".
- Stys, D., Bohlin, R. C., & Goudfrooij, P 2004, STIS ISR 2004, "Time Dependent Sensitivity of the CCD and MAMA First-Order Modes"

## **Appendix A: Photometric Measurements**

Unless otherwise noted all data was taken with gain=4, which was assumed to correspond to 4.08 e<sup>-</sup> per DN.

**Table 15.** Selected Photometric measurements for BD  $-11^{\circ}3759$ 

Data set	Texp	Date	Filter	Instrumental Mag. Gain = 4	
				118.32 pix	157.76 pix
(sec)					
o5ja04050	0.6	2000-07-15	F28X50LP	-14.334	-14.342
o5ja04060	0.6	2000-07-15	F28X50LP	-14.350	-14.360
o5ja04070	0.6	2000-07-15	F28X50LP	-14.327	-14.335
o5ja04080	0.6	2000-07-15	F28X50LP	-14.329	-14.338
mean				-14.335	-14.344
o5ja04010	6.0	2000-07-15	F28X50LP	-14.330	-14.340
o5ja04020	6.0	2000-07-15	F28X50LP	-14.333	-14.342
o5ja04030	6.0	2000-07-15	F28X50LP	-14.332	-14.341
o5ja04040	6.0	2000-07-15	F28X50LP	-14.334	-14.343
mean				-14.332	-14.342
o5ja04090	0.4	2000-07-15	50CCD	-14.555	-14.569
o5ja040a0	0.4	2000-07-15	50CCD	-14.560	-14.569
o5ja040b0	0.4	2000-07-15	50CCD	-14.549	-14.555
o5ja040c0	0.4	2000-07-15	50CCD	-14.557	-14.566
mean				-14.555	-14.565
o5ja040d0	4.0	2000-07-15	50CCD	-14.546	-14.555
o5ja040e0	4.0	2000-07-15	50CCD	-14.549	-14.558
o5ja040f0	4.0	2000-07-15	50CCD	-14.537	-14.545
o5ja040g0	4.0	2000-07-15	50CCD	-14.543	-14.552
mean				-14.544	-14.553

**Table 16.** Photometric measurements for G158-100.

Data set	Texp	Date	Filter	Instrumental Mag. Gain = 4	
				118.32 pix	157.76 pix
(sec)					
o49q01020	240	1997-10-24	F28X50LP	-9.179	-9.185
o49q01030	240	1997-10-24	F28X50LP	-9.172	-9.178
mean				-9.176	-9.182

**Table 17.** Photometric measurements for CPD  $-60^{\circ}7585$  (=SAO 255271 = TYC 9118 576 1)

Data set	Texp	Date	Filter	Instrumental Mag. Gain = 4	
				118.32 pix	157.76 pix
o69c02030	20.0	2000-08-13	F28X50LP	-13.767	-13.771
o69c02060	20.0	2000-08-13	F28X50LP	-13.768	-13.772
o69c02090	20.0	2000-08-13	F28X50LP	-13.771	-13.775
o69c020c0	20.0	2000-08-13	F28X50LP	-13.763	-13.767
mean				-13.767	-13.771
o69c020q0	10.0	2000-08-13	50CCD	-14.503	-14.507
o69c020s0	10.0	2000-08-13	50CCD	-14.501	-14.504
o69c020u0	10.0	2000-08-13	50CCD	-14.507	-14.510
o69c020w0	10.0	2000-08-13	50CCD	-14.501	-14.504
mean				-14.503	-14.506

**Table 18.** Photometric measurements for CPD  $-35^{\circ}9181$  A (=HIP 109149).

Data set	Texp	Date	Filter	Instrumental Magnitude Gain = 4		
				39.4 pix	118.32 pix	157.76 pix
o6h3020k0	6.40	2001-08-25	F28X50LP	-13.948	-14.011	-14.014
o6h3020n0	6.40	2001-08-25	F28X50LP	-13.932	-13.996	-14.001
o6h3020q0	6.40	2001-08-25	F28X50LP	-13.946	-14.009	-14.013
o6h3020t0	6.40	2001-08-25	F28X50LP	-13.931	-13.995	-14.000
o6h3020u0	51.2	2001-08-25	F28X50LP	-13.921	-14.015	-14.020
mean				-13.936	-14.005	-14.010
o6h302050	3.20	2001-08-25	50CCD	-14.424	-14.473	-14.475
o6h302080	3.20	2001-08-25	50CCD	-14.427	-14.477	-14.479
o6h3020b0	3.20	2001-08-25	50CCD	-14.417	-14.467	-14.469
o6h3020e0	3.20	2001-08-25	50CCD	-14.420	-14.471	-14.473
o6h3020f0	25.6	2001-08-25	50CCD	-14.419	-14.469	-14.473
mean				-14.421	-14.471	-14.474

**Table 19.** Photometric Measurements for WD 310–688

Data set	Texp	Date	Filter	Instrumental Magnitude Gain = 4		
				(sec)	39.4 pix	118.32 pix
o69c01030	40.0	2000-09-15	F28X50LP	-11.952	-11.993	-11.999
o69c01060	40.0	2000-09-15	F28X50LP	-11.948	-11.989	-11.997
o69c01090	40.0	2000-09-15	F28X50LP	-11.949	-11.991	-11.997
o69c010c0	40.0	2000-09-15	F28X50LP	-11.942	-11.983	-11.989
mean				-11.948	-11.989	-11.996
o69c010q0	10.0	2000-09-15	50CCD	-13.263	-13.284	-13.284
o69c010s0	10.0	2000-09-15	50CCD	-13.268	-13.290	-13.292
o69c010u0	10.0	2000-09-15	50CCD	-13.268	-13.290	-13.289
o69c010w0	10.0	2000-09-15	50CCD	-13.271	-13.292	-13.292
mean				-13.268	-13.289	-13.289

**Table 20.** Photometric Measurements for GRW +70°5824

Data set	Texp	Date	Filter	Instrumental Magnitude Gain = 4		
				(sec)	39.4 pixels	59.0 pixels
o5ja010t0	22.0	1999-10-21	50CCD	-11.987	-11.998	-12.006
o5ja010u0	22.0	1999-10-21	50CCD	-11.991	-12.002	-12.012
o5ja010v0	22.0	1999-10-21	50CCD	-11.979	-11.991	-12.001
o5ja010w0	22.0	1999-10-21	50CCD	-11.990	-12.002	-12.011
mean				-11.987	-11.998	-12.008
o5ja01110	8.0	1999-10-21	F28X50LP	-10.513	-10.535	-10.557
o5ja010x0	8.0	1999-10-21	F28X50LP	-10.524	-10.539	...
o5ja010y0	8.0	1999-10-21	F28X50LP	-10.523	-10.534	...
o5ja010z0	8.0	1999-10-21	F28X50LP	-10.522	-10.532	...
o5ja01100	8.0	1999-10-21	F28X50LP	-10.517	-10.525	...
mean				-10.520	-10.533	-10.557

**Table 21.** Photometric Measurements for GD 71

Data set	Texp	Date	Filter	Inst. mag. Gain = 4
	(sec)			39.4 pixels
o4a507010	0.6	1997-10-04	50CCD	-11.949
o4a507060	1.0	1997-10-04	F28X50LP	-10.204

**Table 22.** Standard Star F28X50OII measurements.

Star	Data set	Texp	Date	Gain	Instrumental Mag.			
					5 pix	19.7 pix	39.4 pix	59 pix
AGK +81°266	o60n02010	20.0	2000-01-10	1	-9.147	-9.282	-9.324	-9.322
	o60n02020	20.0	2000-01-10	1	-9.172	-9.307	-9.342	-9.339
	o60n02030	20.0	2000-01-10	1	-9.156	-9.294	-9.340	-9.323
	o60n02040	20.0	2000-01-10	1	-9.174	-9.308	-9.356	-9.375
mean	.	.	.	.	-9.162	-9.298	-9.341	-9.340
AGK +81°266	o69l01010	90.0	2000-10-24	4.08	-7.681	-7.800	-7.840	-7.846
	o69l02010	90.0	2001-01-29	4.08	-7.690	-7.802	-7.844	-7.845
	o69l03010	90.0	2001-04-01	4.08	-7.668	-7.799	-7.832	-7.843
	o69s13010	90.0	2000-09-01	4.08	-7.665	-7.784	-7.825	-7.827
	o69s14010	90.0	2000-11-07	4.08	-7.687	-7.802	-7.841	-7.841
	o69s15010	90.0	2001-01-01	4.08	-7.675	-7.794	-7.829	-7.832
	o69s16010	90.0	2001-03-02	4.08	-7.670	-7.802	-7.840	-7.849
	o69s17010	90.0	2001-05-11	4.08	-7.639	-7.764	-7.805	-7.806
mean					-7.672	-7.793	-7.832	-7.836
GRW +70°5824	o5ja01170	600.	1999-10-21	4.08	-6.268	-6.404	-6.443	-6.442
Feige 34	o3zf02050	27.5	1997-05-24	4.08	-8.456	-8.569	-8.603	-8.600
	o3zf02060	25.0	1997-05-24	4.08	-8.457	-8.566	-8.596	-8.590
	o3zf02070	25.0	1997-05-24	4.08	-8.390	-8.507	-8.541	-8.547
	o3zf02080	25.0	1997-05-24	4.08	-8.448	-8.561	-8.592	-8.588
	mean excluding o3zf02070				-8.523	-8.557	-8.597	-8.592

**Table 23.** Standard Star F28X50OIII Measurements.

star	data set	texp (sec)	Date	gain	Instrumental Mag. (gain = 4).			
					5 pix	19.7 pix	39.4 pix	59 pix
GRW +70°5824	o4vg01040	600.0	1998-06-07	4.08	-4.501	-4.609	-4.645	-4.642
	o5ja01160	1062.0	1999-10-21	4.08	-4.464	-4.622	-4.661	-4.643
	mean				-4.483	-4.616	-4.653	-4.643
Feige 34	o3zf02010	601.0	1997-05-24	4.08	-6.113	-6.219	-6.260	-6.272
	o3zf02020	600.0	1997-05-24	4.08	-6.108	-6.216	-6.260	-6.272
	o3zf02030	600.0	1997-05-24	4.08	-6.096	-6.208	-6.249	-6.263
	o3zf02040	660.0	1997-05-24	4.08	-6.080	-6.187	-6.231	-6.244
	mean				-6.099	-6.208	-6.250	-6.263